JACS
JOURNAL OF THE AMERICAN CHEMICAL SOCIETY
pubs.acs.org/JACS
Article

Precision Synthesis of Polysarcosine via Controlled Ring-Opening Polymerization of *N*-Carboxyanhydride: Fast Kinetics, Ultrahigh Molecular Weight, and Mechanistic Insights

Shuo Wang, Ming-Yuan Lu, Si-Kang Wan, Chun-Yan Lyu, Zi-You Tian, Kai Liu, and Hua Lu*

Cite This: *J. Am. Chem. Soc.* 2024, 146, 5678−5692

ABSTRACT: The rapid and controlled synthesis of high-molecular-weight (HMW) polysarcosine (pSar), a potential polyethylene glycol (PEG) alternative, via the ring-opening polymerization (ROP) of *N*-carboxyanhydride (NCA) is rare and challenging. Here, we report the well-controlled ROP of sarcosine NCA (Sar-NCA) that is catalyzed by various carboxylic acids, which accelerate the polymerization rate up to 50 times, and enables the robust synthesis of pSar with an unprecedented ultrahigh molecular weight (UHMW) up to 586 kDa (DP ∼ 8200) and exceptionally narrow dispersity (*Đ*) below 1.05. Mechanistic experiments and density functional theory calculations together elucidate the role of carboxylic acid as a bifunctional catalyst that significantly facilitates proton transfer processes and avoids charge separation and suggest the ring opening of NCA, rather than decarboxylation, as the rate-determining step. UHMW pSar demonstrates improved thermal and mechanical properties over the low-molecular-weight counterparts. This work provides a simple yet highly efficient approach to UHMW pSar and generates a new fundamental understanding useful not only for the ROP of Sar-NCA but also for other NCAs.

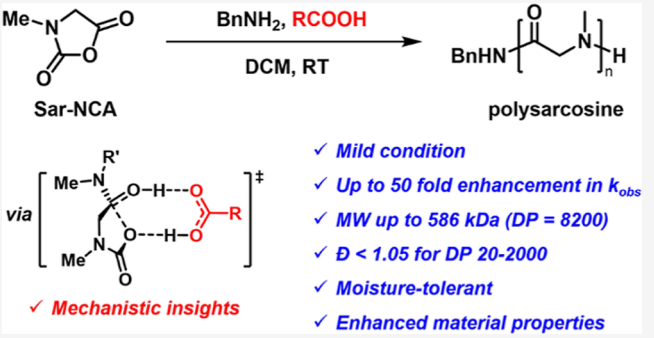

1. INTRODUCTION

Polysarcosine (pSar) is a nonionic water-soluble polypeptoid with the biogenic amino acid sarcosine (*N*-methylglycine) as the repeating unit. Being comparable in flexibility, hydrophilicity, low cytotoxicity, and excellent antibiofouling properties to polyethylene glycol (PEG), pSar has been considered a potential alternative to PEG.[1−3] For example, the pSar-interferon conjugate exhibits a similar in vivo circulation half-life to the PEG-interferon conjugate of the same size while being more potent in inhibiting tumor growth.[4] pSar-functionalized nanoparticles (LNPs) have also been reported for mRNA delivery, which led to lower immunogenicity and higher delivery efficiency over conventional PEGylated LNPs.[5,6] Additionally, pSar has been frequently used as the hydrophilic composition of nonionic surfactants or amphiphilic block copolymers for the purpose of disease diagnosis and treatment.[7−14]

pSar is typically synthesized through the ring-opening polymerization (ROP) of sarcosine *N*-carboxyanhydride (Sar-NCA)[15−30] or *N*-thiocarboxyanhydride (Sar-NTA).[31−36] However, existing Sar-NCA polymerization methods often require strictly anhydrous conditions, limiting its broader applications and large-scale production. In contrast, Sar-NTA demonstrates better moisture tolerance than Sar-NCA but suffers harsh polymerization conditions due to lower reactivity.[32] Furthermore, the achievable molecular weight (MW) of pSar via current methods is generally limited, with degrees of polymerization (DP) lower than 500 and a maximal MW of ∼35 kDa.[34] As several FDA-approved PEGylated protein drugs are modified with PEG of 40−80 kDa,[37] it is crucial to develop a rapid and robust Sar-NCA polymerization method capable of achieving a broader and higher MW coverage.

The elucidation of the polymerization mechanism plays a pivotal role in the development of new methodologies.[38] In the case of the ROP of Sar-NCA initiated by primary amines, the chain propagation involves two consecutive steps: the ring-opening amidation reaction wherein the amine attacks the carbonyl group of NCA, and the subsequent decarboxylation reaction of the carbamic acid intermediate (Figure 1A).[21] However, insights into the reaction details, such as the proton transfer process[39] and rate-determining step (RDS), were surprisingly rare.[40] Essentially, proton transfer is crucial in both

Received: December 28, 2023
Revised: January 29, 2024
Accepted: January 30, 2024
Published: February 15, 2024

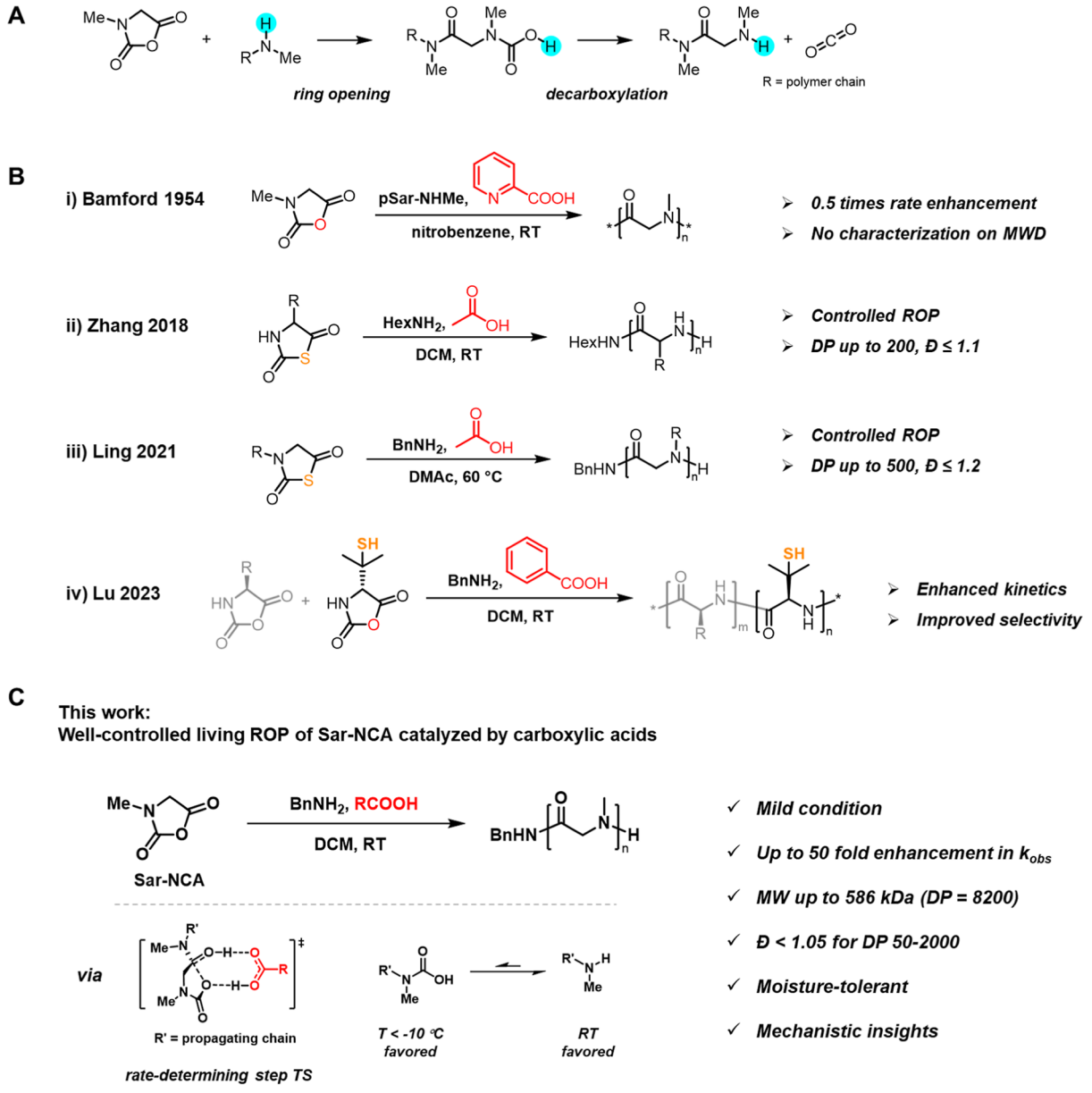

Figure 1. (A) Two consecutive steps for chain propagation of Sar-NCA ROP. (B) Previous works on carboxylic acid-catalyzed ROP of NCAs or NTAs. (C) Carboxylic acid-catalyzed ROP of Sar-NCA studied in this work.

the amidation and decarboxylation processes but often faces geometric constraints in intramolecular cases, leading to high activation energies due to unfavorable transition states (TSs).[41,42] On the other hand, intermolecular proton transfer catalysts can overcome the geometric constraints' limitations and reduce activation energy.[43−47] In a recent work on the ROP of proline NCA (Pro-NCA), Lu et al. noticed a remarkable acceleration effect by simply adding water as the cosolvent.[48] Through experiments and density functional theory (DFT) calculations, they ascribed this unexpected acceleration to water's ability to act as a proton shuttle, which effectively lowered the energy barriers. Yet, this water-accelerating effect has not been observed in the ROP of other NCAs.

Carboxylic acids are common proton transfer catalysts, possessing both an acidic proton donor site and a basic carbonyl proton acceptor site within a conjugated π system.[49,50] This enables the carboxylic group to accept an external proton and donate its own proton via a concerted TS without compromising electronic neutrality.[51−53] In this regard, we envision that introducing carboxylic acids as proton transfer catalysts into the ROP of Sar-NCA holds great potential for enhancing the polymerization rate. In an early study conducted by Ballard and Bamford in 1954, the addition of pyridine-2-carboxylic acid to the ROP of Sar-NCA in nitrobenzene was found to increase the polymerization rate by ~0.5 times (Figure 1B).[54] Although this work had a limited polymerization rate and lacked characterization on molecular weight distribution (MWD) of the pSar product, it did provide the first experimental evidence supporting the use of carboxylic acids in NCA polymerization. More recently, both the Zhang et al.'[36] and Ling et al.'[34] laboratories reported the carboxylic acid-promoted ROP of NTA and *N*-substituted NTA, respectively (Figure 1B). Remarkable rate acceleration was observed in both ROP systems after adding carboxylic acids, which was attributed to the promoted removal of carbonyl

https://doi.org/10.1021/jacs.3c14740
J. Am. Chem. Soc. 2024, 146, 5678−5692

Table 1. Benzoic Acid-Catalyzed ROP of Sar-NCA[a]

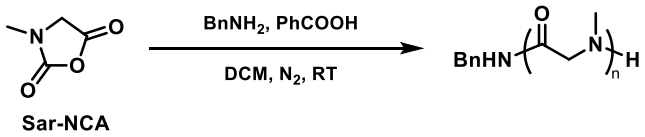

entry	$[M]_0$ (M)	$[M]_0/[I]_0/[A]_0$	time	M_n^{cal} (kDa)[b]	M_n^{obt} (MALLS) (kDa)[c]	$Đ$ (MALLS)[c]	M_n^{obt} (PS) (kDa)[d]	$Đ$ (PS)[d]
1	0.2	50/1/0	2 h	3.7	5.2	1.01		
2	0.2	20/1/5	<15 min	1.5	1.6	<1.01	1.8	1.16
3	0.2	50/1/5	<15 min	3.7	4.3	1.01	5.8	1.04
4	0.2	100/1/5	<15 min	7.2	8.9	<1.01	11.8	1.03
5	0.2	200/1/5	17 min	14.3	17.5	1.01	25.0	1.02
6	0.2	500/1/5	<1.5 h	35.6	41.6	1.01	57.7	1.02
7	0.2	1000/1/5	2.5 h	71.2	74.3	<1.01	105.7	1.03
8	0.4	1000/1/5	1.5 h	71.2	78.6	1.01		
9	0.4	1500/1/5	1.5 h	106.7	111.8	<1.01	146.2	1.04
10	0.4	2000/1/5	2.5 h	142.3	136.9	<1.01	222.3	1.04
11	0.4	2000/1/0	13 h	142.3	84.5	1.14	88.1	1.37
12	0.4	5000/1/5	16.5 h	355.5	340.6	1.02	391.4	1.16
13	0.8	10,000/1/5	16.5 h	710.9			414.1	1.31

[a]Conversions of monomer were monitored by infrared spectroscopy (IR) and were all above 95% except entry 11. [b]Calculated number-average molecular weight based on feed ratios. [c]Determined by SEC equipped with a MALLS detector using dimethylformamide containing 0.1 M LiBr as the mobile phase; the dn/dc (658 nm) value of pSar was measured as 0.079 mL/g. [d]Determined by SEC relative to polystyrene standards.

sulfide. Furthermore, we recently discovered that the addition of benzoic acid in the ROP of unprotected penicillamine NCA (Pen-NCA) not only accelerated the polymerization rate but also improved the selectivity of polymerization over monomer isomerization (Figure 1B).[55] During the preparation of this work, Zhang/Xuan and Cheng/Song independently reported similar acceleration.[56,57] These successes motivated us to comprehensively investigate the role of carboxylic acids in the polymerization process of Sar-NCA.

Herein, we report a systematic study on carboxylic acid-catalyzed primary amine-initiated well-controlled ROP of Sar-NCA. The system enables the fast and robust synthesis of pSar with an unprecedented high MW up to 586 kDa (DP ~ 8200), 16 times higher than the previous record, and exceptionally narrow dispersity ($Đ$) below 1.05 (Figure 1C). Moreover, the polymerization can be carried out under mild and ambient conditions without dry solvents, Schlenk line, or glovebox operations. DFT calculations combined with mechanistic experiments show that the ring-opening step of carboxylic acid-catalyzed Sar-NCA ROP proceeds through a stepwise nucleophilic addition−elimination process, with the elimination of the tetrahedral intermediate as the RDS. The carboxylic acid reduces the charge separation during the reaction through hydrogen-bond bridging and assists the proton transfer process in the form of a proton shuttle. High-molecular-weight pSar shows excellent thermal stabilities and good processability to form high-strength transparent films.

2. RESULTS AND DISCUSSION

2.1. Benzoic Acid-Catalyzed ROP of Sar-NCA. In our initial attempt, benzoic acid was used as the catalyst, and the benzylamine-mediated ROP of Sar-NCA was performed in dry dichloromethane (DCM) in a glovebox at room temperature. At an initial monomer concentration ($[M]_0$) of 0.2 M, we found that the reaction system with a feeding $[M]_0/[I]_0/[A]_0$ (the initial concentration of monomer, initiator, and carboxylic acid catalyst, respectively) ratio of 50:1:5 achieved complete monomer conversion within 15 min (monitored by infrared spectroscopy); in contrast, the control group without benzoic acid required 2 h to reach a full conversion (Table 1, entry 1 and 3). Size exclusion chromatography (SEC) characterization of the acid-catalyzed polymerization exhibited a sharp and symmetrical peak (Figure 2A), whose narrow $Đ$ of 1.01 and an obtained number-average molecular weight (M_n^{obt}) of 4.3 kDa, close to the calculated theoretical M_n (M_n^{cal} 3.7 kDa), were determined by an SEC-coupled multiangle laser light scattering (MALLS) detector. Analysis of the same polymer based on calibration of polystyrene (PS) standard samples gave M_n^{obt} and $Đ$ of 5.8 kDa and 1.04, respectively. Matrix-assisted laser desorption time-of-flight (MALDI-TOF) mass spectrometry confirmed the good end-group fidelity of the acid-catalyzed polymerization, with the α- and ω-end of the pSar product (Table 1, entry 3) exclusively in the form of $C_6H_5CH_2NH-$ and H−, respectively (Figure 2B).

With the encouraging initial results, we conducted systemic ROP studies with different $[M]_0/[I]_0$ ratios ranging from 20:1 to 1000:1 at a fixed $[I]_0/[A]_0$ ratio of 1:5, which gave excellent results with a $Đ$ below 1.05 and linearly increased M_n^{obt} close to M_n^{cal} (Table 1, entry 2−7; Figure 2C,D). Raising $[M]_0$ from 0.2 to 0.4 M effectively accelerated the reaction without losing control over MW (Table 1, entry 7 and 8). Notably, under the catalysis of benzoic acid, the polymerization with an $[M]_0/[I]_0$ of 2000 was completed within 2.5 h, producing pSar with an M_n^{obt} of 136.9 kDa (M_n^{cal} = 142.3 kDa, Table 1, entry 10); in contrast, the same reaction without acid catalysis rendered only ~75% monomer conversion even after overnight reaction, affording pSar with a severely lower M_n^{obt} and a tailing SEC trace (Table 1, entry 11; Figures S1 and S2). At a further increased $[M]_0/[I]_0$ of 5000, remarkably, the polymerization still maintained excellent control (M_n^{obt} 340.6 kDa vs M_n^{cal} 355.5 kDa) with a completed monomer conversion in 16.5 h (Table 1, entry 12). The upper limit of the system was finally reached at a $[M]_0/[I]_0$ of 10,000:1 ($[M]_0$ = 0.8 M), producing pSar after overnight reaction with a M_n^{obt} of 414.1 kDa, significantly lower than the M_n^{cal} of 710.9 kDa (Table 1, entry 13; Figure S3). This deviation could be attributed to the trace

https://doi.org/10.1021/jacs.3c14740
J. Am. Chem. Soc. 2024, 146, 5678−5692

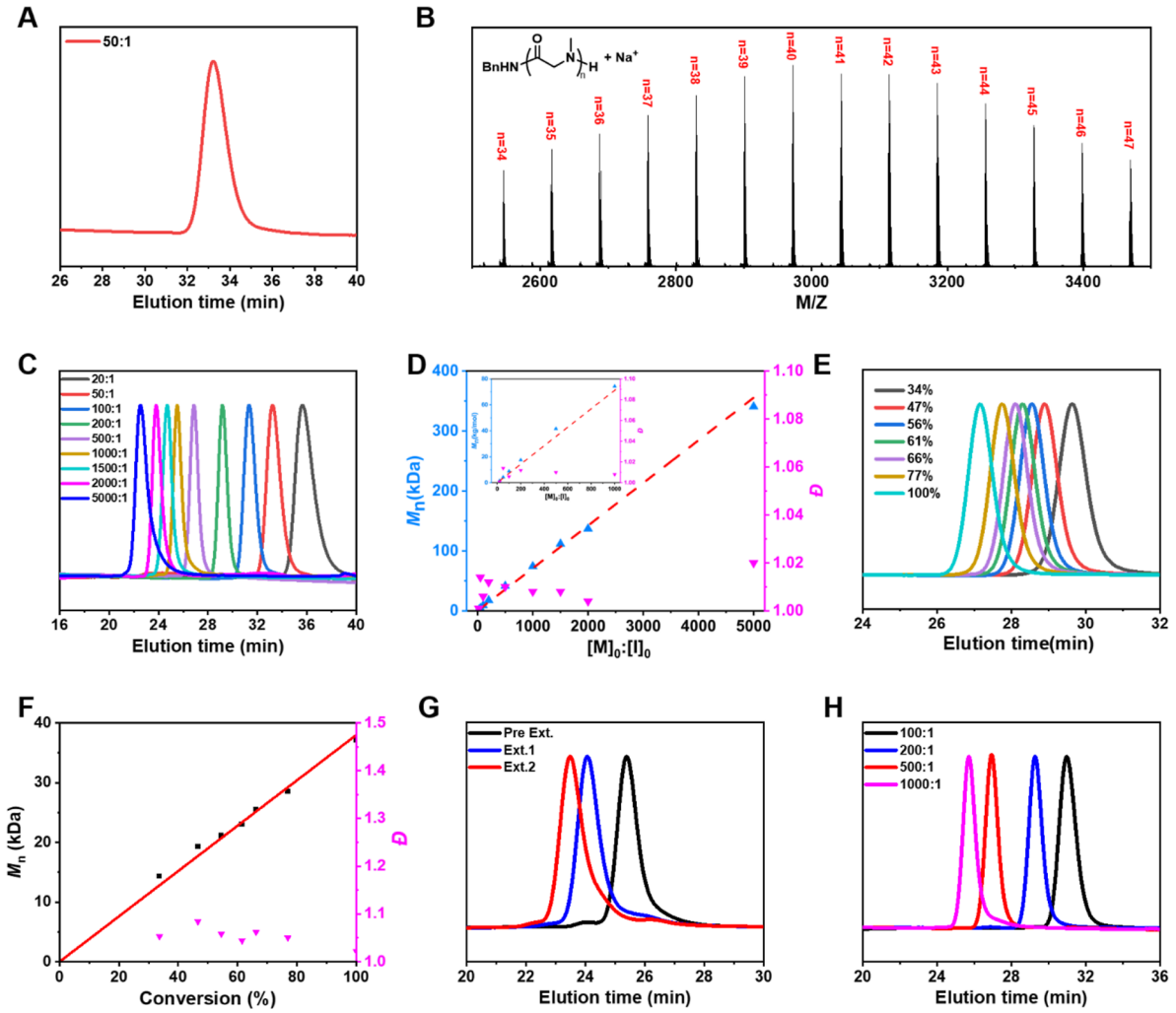

Figure 2. Benzoic acid-catalyzed ROP of Sar-NCA. (A) SEC trace of pSar at the $[M]_0/[I]_0/[A]_0$ ratio of 50:1:5. (B) MALDI-TOF MS spectrum of pSar prepared by $[M]_0/[I]_0/[A]_0$ = 50:1:5. (C) SEC traces of pSar at different $[M]_0/[I]_0$ ratios with $[I]_0/[A]_0$ fixed at 1:5. (D) Plots of M_n and $Đ$ as a function of the $[M]_0/[I]_0$ ratio. (E) SEC traces at different monomer conversions at the $[M]_0/[I]_0/[A]_0$ ratio of 500:1:5. (F) Plots of M_n and $Đ$ as a function of the monomer conversion at the $[M]_0/[I]_0/[A]_0$ ratio of 500:1:5. (G) SEC traces of pSar before and after chain extension. (H) SEC traces at different $[M]_0/[I]_0$ ratios in conventional DCM in an ambient atmosphere.

impurities with initiator activities in the monomer, which, however, was undetectable in the ^{1}H NMR spectrum (Figure S4). To the best of our knowledge, the rapid and controlled synthesis of pSar with a DP of 600−5000 has never been reported.

Next, we examined the living character, i.e., chain growth pattern and chain extension, of the benzoic acid-catalyzed ROP of Sar-NCA. At an $[M]_0/[I]_0/[A]_0$ ratio of 500:1:5, the M_n^{obt} of pSar was found to increase linearly with monomer conversion, which was consistent with the characteristics of controlled chain growth polymerization (Figure 2E,F). Furthermore, to a fully converted $[M]_0/[I]_0/[A]_0$ ratio of 1000:1:5 system (Figure 2G, pre-ext., M_n^{obt} 76.7 kDa vs M_n^{cal} 71.2 kDa), adding another 1000 equiv of monomer reached full conversion within 4 h, with the SEC characterization revealing a complete shift of the product peak toward the higher MW region (Figure 2G, ext.1, M_n^{obt} 139.3 kDa vs M_n^{cal} 142.3 kDa). The same chain extension could be repeated with good control of MW (Figure 2G, ext.2, M_n^{obt} 192.8 kDa vs M_n^{cal} 213.3 kDa). The $Đ$ of the polymers was kept low during the repeated chain extension courses (Figure 2G, Table S1). Interestingly, when the polymerization was carried out under ambient conditions using HPLC-grade DCM, the controlled MWs were still observed, indicating good moisture and oxygen tolerance upon enhanced reaction rate (Figure 2H, Table S2).

To investigate the kinetic characters and details of the above benzoic acid-catalyzed ROP, an online Fourier transform infrared (FT-IR) spectrometer was employed to monitor monomer conversions in situ (Figures S5 and S6). First, the $[M]_0/[I]_0$ ratio was fixed at 200:1, and control experiments were conducted for polymerization systems with and without the addition of an acid catalyst. Under the same conditions, the ROP with an $[M]_0/[I]_0/[A]_0$ ratio of 200:1:5 reached 95% conversion within 17 min, while the reaction at the $[M]_0/[I]_0/[A]_0$ ratio of 200:1:0 took 5 h (Figure 3A). The 200:1:5 group presented typical first-order kinetics, and $\ln([M]_0/[M])$ had a good linear relationship with the reaction time (R^2 = 0.9989), through which the apparent first-order rate constant k_{obs} was calculated as $(30.9 \pm 0.3) \times 10^{-4}$ s^{-1} (Figure 3B). In contrast, the 200:1:0 group showed a sluggish, multiple-stage kinetic profile with first a slow induction period followed by a self-accelerating pattern and reaching a steady state with first-order kinetics (Figure S7). The k_{obs} of the steady stage was then calculated as $(1.95 \pm 0.02) \times 10^{-4}$ s^{-1}, 1/15th of the catalyzed

https://doi.org/10.1021/jacs.3c14740
J. Am. Chem. Soc. 2024, 146, 5678−5692

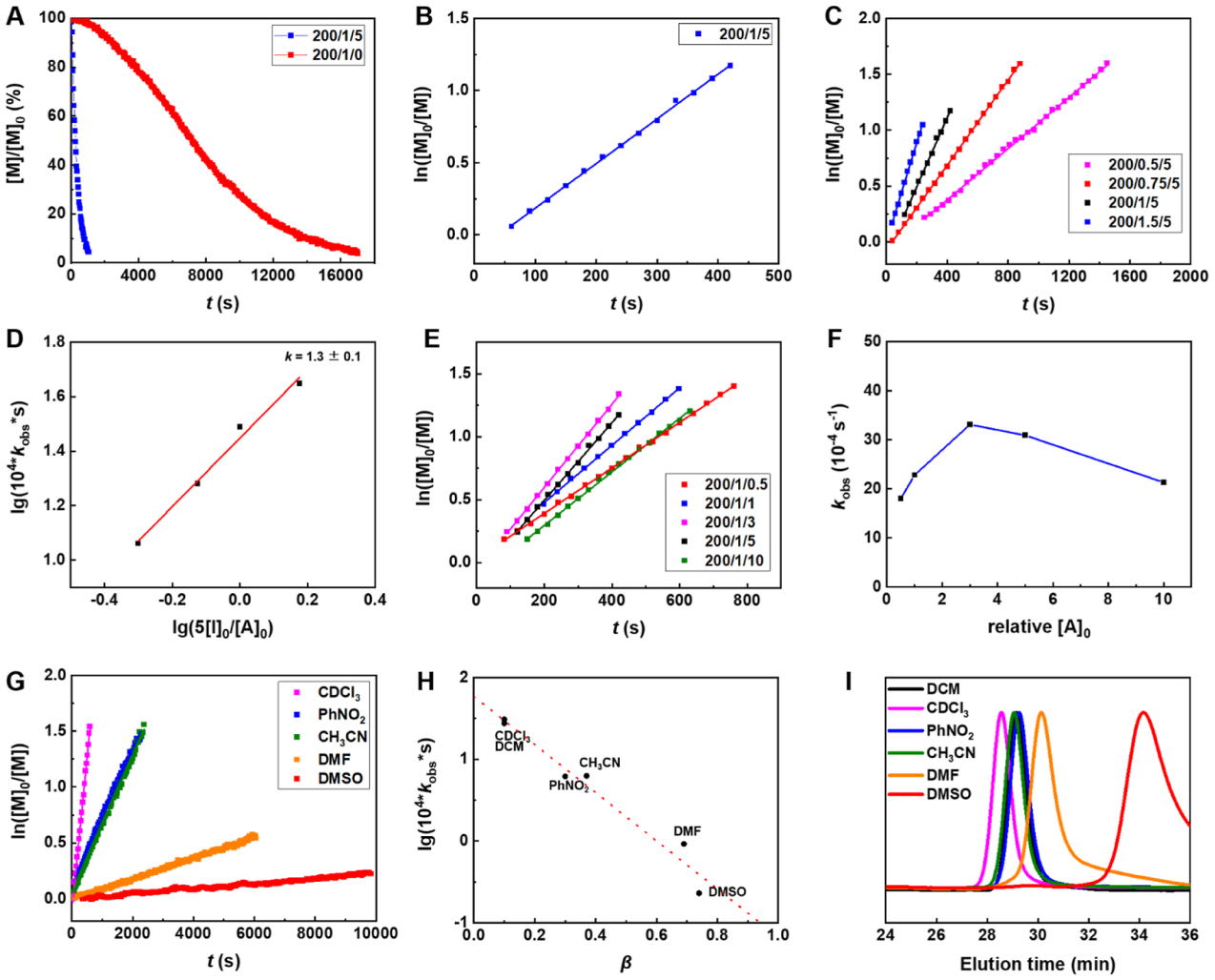

Figure 3. Kinetic study and solvent effect of carboxylic acid-catalyzed ROP of Sar-NCA. (A) Kinetic plots of $[M]/[M]_0$ versus time, with or without the catalyst benzoic acid at the $[M]_0/[I]_0$ ratio of 200:1. (B) Kinetic plot of $\ln([M]_0/[M])$ versus time at the $[M]_0/[I]_0/[A]_0$ ratio of 200:1:5. (C) Kinetic plots of $\ln([M]_0/[M])$ versus time with varied initiator equivalent at the $[M]_0/[A]_0$ ratio of 200:5. (D) Plot of k_{obs} obtained from (C) versus $[I]_0$ and the linear fitting (red line, R^2 = 0.988) of the data. (E) Kinetic plots of $\ln([M]_0/[M])$ versus time with varied $[A]_0$ equivalent at the $[M]_0/[I]_0$ ratio of 200:1. (F) Plot of k_{obs} obtained from (E) versus $[A]_0$. (G) Kinetic plots of $\ln([M]_0/[M])$ versus time at the $[M]_0/[I]_0/[A]_0$ ratio of 200:1:5 in different solvents. (H) Plot of k_{obs} obtained from (G) versus β. (I) SEC curves of pSar synthesized in different solvents.

group (Figure S8). Next, $[I]_0$ was varied to probe the relationship between k_{obs} and $[I]_0$, and all the ROPs were found to present typical first-order kinetics (Figure 3C, R^2 > 0.998). Plotting $\lg(k_{obs})$ as a function of $\lg([I]_0)$ revealed a linear correlation with a slope of 1.3 (R^2 = 0.988, Figure 3C,D, Table S3). The change of reaction rate with $[A]_0$, however, was not monotonic (Figure 3E,F, Table S3). With $[A]_0$ increased, k_{obs} first increased, reaching a maximum of $(33.1 \pm 0.2) \times 10^{-4}$ s^{-1} at the $[I]_0/[A]_0$ ratio of 1:3 and then slowly decreased with further added $[A]_0$. We reasoned that the excessive carboxylic acid likely decreased the ROP rate through the competing reaction by partially protonating the chain propagating amine (acid−amine equilibrium). Similar effects were seen in cases where strong acids such as HCl, HBF_4, and phosphoric acids were used for controlled ROP of NCAs, leading to significantly sacrificed reactivity, monomer conversion, and/or long induction period.[23,25,58]

Furthermore, the acid-catalyzed ROP was investigated in various solvents such as (deuterated) chloroform, nitrobenzene, acetonitrile, DMF, and DMSO at the feeding $[M]_0/[I]_0/[A]_0$ ratio of 200:1:5 (Table S4). The reactions displayed first-order kinetics in all solvents, among which chloroform showed a comparable k_{obs} with DCM of $(27.6 \pm 0.2) \times 10^{-4}$ s^{-1}. The ROP rates in nitrobenzene and acetonitrile, however, were substantially slower with the k_{obs} being ~6×10^{-4} s^{-1}, one-fifth of that of DCM. ROP in DMF and DMSO demonstrated the slowest rates, with the k_{obs} of $(0.923 \pm 0.004) \times 10^{-4}$ s^{-1} and $(0.230 \pm 0.004) \times 10^{-4}$ s^{-1}, respectively. Interestingly, there was a strong negative correlation between k_{obs} and the Kamlet−Abboud−Taft basicity parameter β[59−61] of the solvents: the larger the β, the slower the reaction rate (Figure 3H). Since β indicated the ability to accept hydrogen bonds, the solvents with a strong Lewis basicity (greater β) tended to compete with substrates interacting with carboxylic acid catalysts via hydrogen bonding, thereby reducing the catalytic activity. The SEC traces of pSar obtained in chloroform, nitrobenzene, and acetonitrile were all symmetric and narrowly distributed, with the M_n^{obt} of pSar obtained in nitrobenzene and acetonitrile showing greater coincidence with M_n^{cal} than that in chloroform. A severe tailing

https://doi.org/10.1021/jacs.3c14740
J. Am. Chem. Soc. 2024, 146, 5678−5692

A

entry	acid	pKa (water)	k_{obs} (10^{-4} s^{-1})	M_n^{obt} (MALLS) (kDa)	Đ (MALLS)	M_n^{obt} (PS) (kDa)	Đ (PS)
1	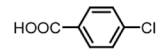	3.99	15.3±0.1	15.5	1.05	23.3	1.02
2	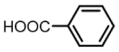	4.20	30.9±0.3	17.5	1.01	25.0	1.02
3	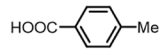	4.37	50.2±0.4	15.3	1.05	23.1	1.02
4	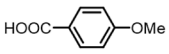	4.47	54.5±0.7	15.9	1.04	23.8	1.02
5	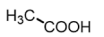	4.76	77.9±0.9	16.2	1.06	24.1	1.02
6	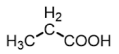	4.87	86.4±1.0	15.5	1.05	23.1	1.02
7	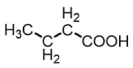	4.82	86.7±1.0	15.8	1.04	23.7	1.02
8		5.05	100.6±1.3	14.7	1.03	21.8	1.02
9	none	-	1.95 ± 0.02	12.7	1.07	13.5	1.26

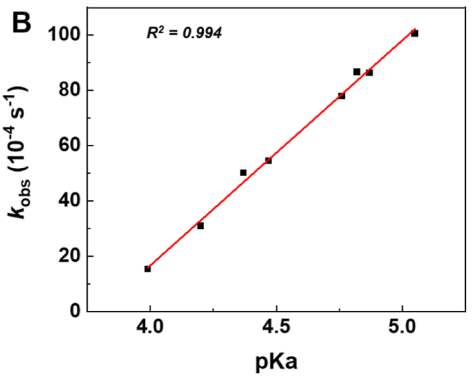

Figure 4. ROP of Sar-NCA catalyzed by different acids. (A) Results of Sar-NCA ROP catalyzed by different carboxylic acids. (B) Plot of k_{obs} versus pK_a values of acids. (C) SEC curves of selected entries from (A).

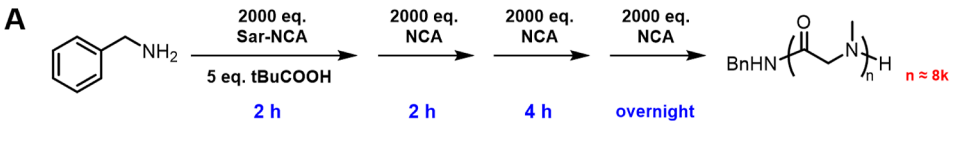

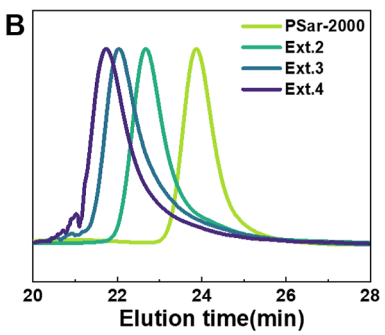

C

Number of blocks	M_n^{cal} (kDa)	M_n^{obt} (MALLS) (kDa)	Đ (MALLS)	M_n^{obt} (PS) (kDa)	Đ (PS)
1	142.2	157.1	< 1.01	210.0	1.05
2	284.4	305.5	< 1.01	350.8	1.16
3	426.6	-	-	466.2	1.26
4	568.7	-	-	586.4	1.25

Figure 5. Chain extension catalyzed by tBuCOOH for the synthesis of HMW pSar. (A) Consecutive chain extension experiment. (B) SEC traces of chain extension products. (C) M_n and Đ of pSar products calculated from SEC.

in the SEC peak was observed for the ROP in DMF, and the reaction in DMSO produced pSar with a much smaller M_n^{obt} than expected (Figure 3I, Table S4). Overall, DCM is the best solvent, with the fastest kinetics and excellent control on MW.

2.2. Influence of Carboxylic Acidity on Sar-NCA ROP. Next, various carboxylic acids with different acidities were explored for the ROP of Sar-NCA at a fixed $[M]_0/[I]_0/[A]_0$ ratio of 200:1:5 (Figure 4). Despite the difference in chemical structure, all the acid catalysts rendered first-order kinetics of the ROP against the monomer, from which k_{obs} was calculated (Figures 4A and S9). Interestingly, a good linear correlation (R^2 = 0.994) between k_{obs} and the pK_a[62] of carboxylic acids was found—the weaker the acidity, the higher the k_{obs} (Figure 4B). Among the acids studied, pivalic acid showed the highest k_{obs}, reaching (100.6 ± 1.3) × 10^{-4} s^{-1}, 3 times that of benzoic acid and more than 50 times that of the acid-free control group. Moreover, all pSar synthesized by carboxylic acid-catalyzed ROP showed symmetrical and narrow SEC peaks, in sharp contrast with the ROP without acid exhibiting significant tailing in the SEC trace (Figure 4C).

2.3. Pivalic Acid-Catalyzed Consecutive Chain Extensions for the Synthesis of Ultrahigh Molecular Weight (UHMW) pSar. Based on the above screening, we identified pivalic acid as a more efficient catalyst than benzoic acid, which could potentially further boost the polymerization kinetics and lead to the construction of pSar with higher MWs. To this end,

https://doi.org/10.1021/jacs.3c14740
J. Am. Chem. Soc. 2024, 146, 5678−5692

Table 2. ROP of NBG-NCA and Synthesis of (Multi) Block Copolymers[a]

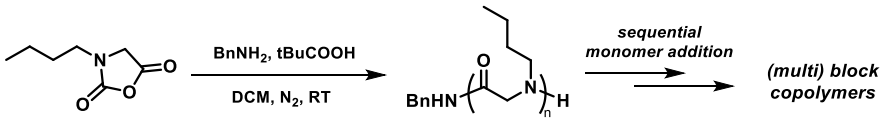

entry	polymer	$[M]_0$ (M)	time	M_n^{cal} (kDa)[b]	M_n^{obt} (kDa)[c]	$Đ$[c]
1	NBG_{20}	0.4	15 min	2.4	2.8	1.12
2	NBG_{200}	0.4	1 h	22.7	32.6	1.02
3	NBG_{1000}	0.8	17 h	113.3	149.5	1.04
4	NBG_{2000}	0.8	24 h	226.4	254.1	1.08
5−1[d]	NBG_{20}-*b*-Sar_{400}	0.4	1 h[g]	30.8	40.5	1.02
5−2[e]	NBG_{20}-*b*-Sar_{400}-*b*-NBG_{20}	0.02	15 h[g]	33.1	44.6	1.02
6[f]	NBG_{1000}-*b*-Sar_{1000}	0.4	3.5 h[g]	184.3	241.6	1.09

[a]$[I]_0/[A]_0$ was fixed as 1:5 for all entries. Conversions of monomer were monitored by IR and were all above 95%. [b]Calculated number-average molecular weight based on feed ratios. [c]Determined by SEC relative to polystyrene standards. [d]Reaction solution of entry 1 was directly used for block copolymer synthesis via sequential monomer addition. [e]NBG-NCA was added to the solution of entry 5−1. [f]Reaction solution of entry 3 was directly used for block copolymer synthesis via sequential monomer addition. [g]Time for the full conversion (>95%) of monomer for the last block.

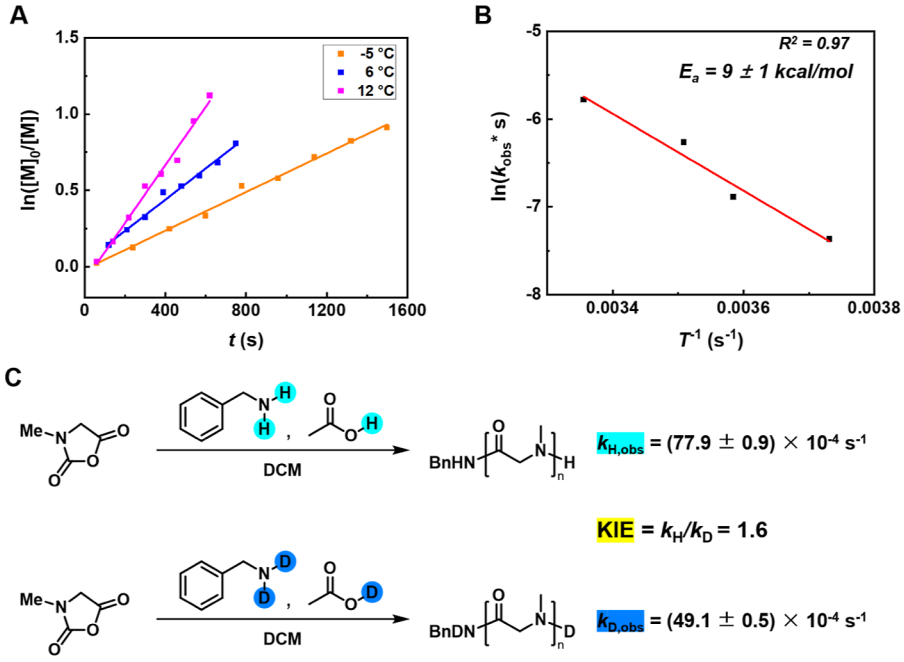

Figure 6. (A) Kinetic plot of $\ln([M]_0/[M])$ versus time under different temperatures at the $[M]_0/[I]_0/[A]_0$ ratio of 200:1:5. (B) Arrhenius plot of $\ln(k_{obs})$ versus T^{-1} and the linear fitting. (C) Kinetic isotopic effect in acetic acid-catalyzed ROP with the $[M]_0/[I]_0/[A]_0$ ratio of 200:1:5.

consecutive chain extensions, each with 2000 equiv of Sar-NCA relative to the initiator, were conducted (Figure 5A). IR monitoring indicated that it took only 2 h for the first two feeds to reach full monomer conversion, and the third feed required a slightly longer time of 4 h. The last feed needed overnight reaction to consume all monomers. SEC characterization showed that each chain extension led to an overall shift of the chromatogram peak curve to the high MW region (Figure 5B). A UHMW pSar with a 586 kDa MW (DP ∼ 8200, $Đ$ = 1.25) was obtained, in good agreement with the theoretical MW and 16 times higher than the previous highest record (Figure 5C). Note that tailing peaks were observed for the extension of the last two blocks, likely the result of chain termination by S_N2 reaction between amine living center and DCM solvent, which was supported by a small-molecule model reaction (Figures S10−S14). Additionally, trace impurities with initiator activity in the monomer may also contribute to the tailing effect.

2.4. Pivalic Acid-Catalyzed ROP of *N*-^{n}Bu Glycine NCA and the Synthesis of (Multi) Block Copolymers. To assess the generality of this method, we subsequently investigated the pivalic acid-catalyzed ROP of another N-substituted NCA (NNCA), namely, *N*-^{n}Bu glycine NCA (NBG-NCA). By following the same condition of Sar-NCA, NBG-NCA was smoothly polymerized in a controlled manner with relatively fast kinetics (Table 2, entry 1−4), albeit slower than the less bulky Sar-NCA. Poly(*N*-^{n}Bu glycine) (PNBG or NBG_n) with a DP ranging from 20 to 2000 was obtained in 15 min to 24 h with narrow $Đ$ (Figure S15), and the good end-group fidelity of NBG_{20} was confirmed by MALDI-TOF MS (Figure S16). Notably, HMW PNBG with a DP over 500, like pSar, was also rarely reported by precedent publications, which echoes the robustness and high efficiency of our method. More importantly, the chain ends of these PNBGs remained living after full conversion of monomers, greatly facilitating the synthesis of (multi) block copolypeptoids. As demonstrated in

https://doi.org/10.1021/jacs.3c14740
J. Am. Chem. Soc. 2024, 146, 5678−5692

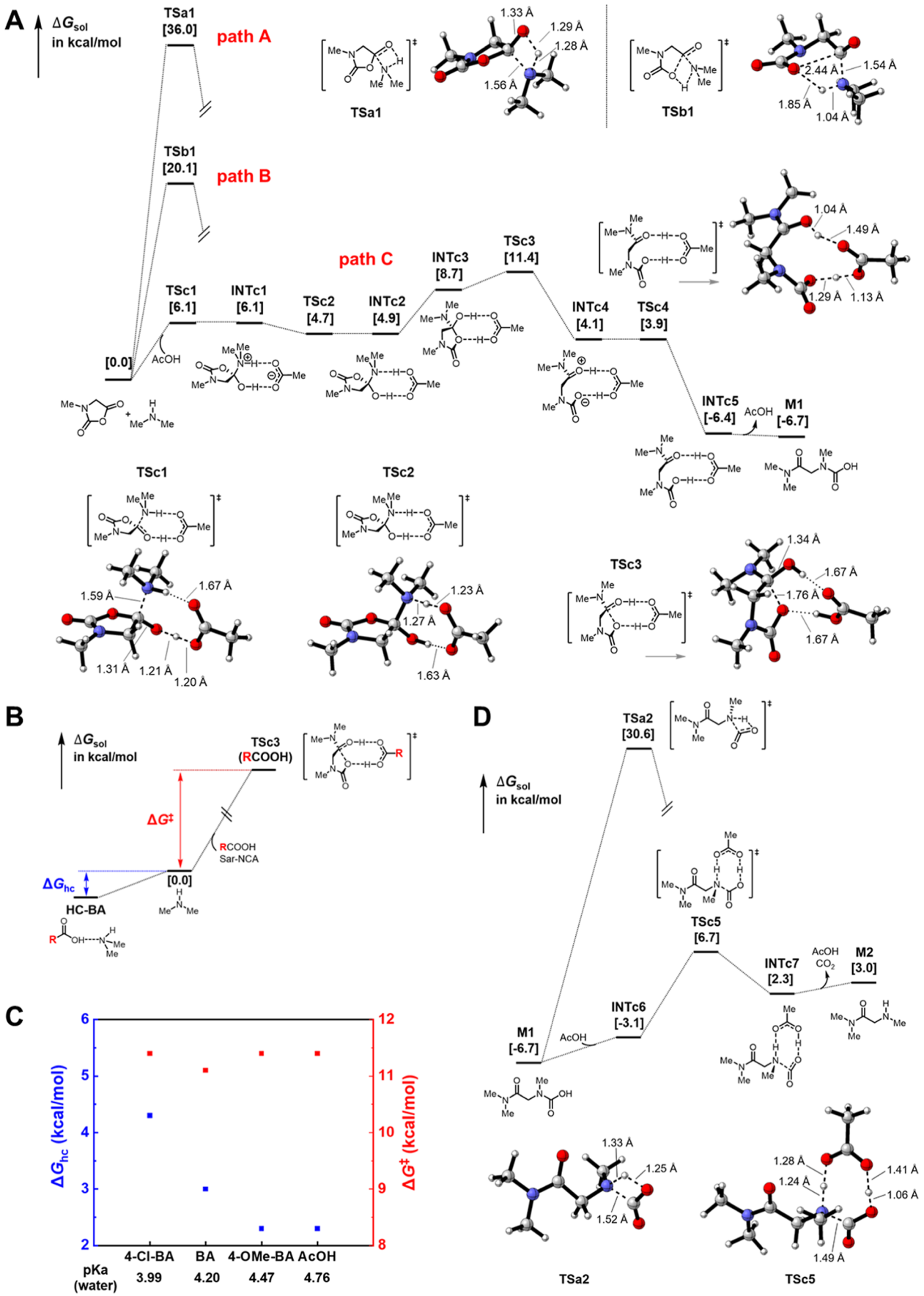

Figure 7. (A) Computed PES for pathways of the ring-opening step. (B) Calculation on the ring-opening step catalyzed by different catalysts. (C) Dependence of ΔG_{hc} and $\Delta G^{\ddagger}$ on the structure and acidity of catalysts. (D) Computed PES for pathways of the decarboxylation step.

https://doi.org/10.1021/jacs.3c14740
J. Am. Chem. Soc. 2024, 146, 5678−5692

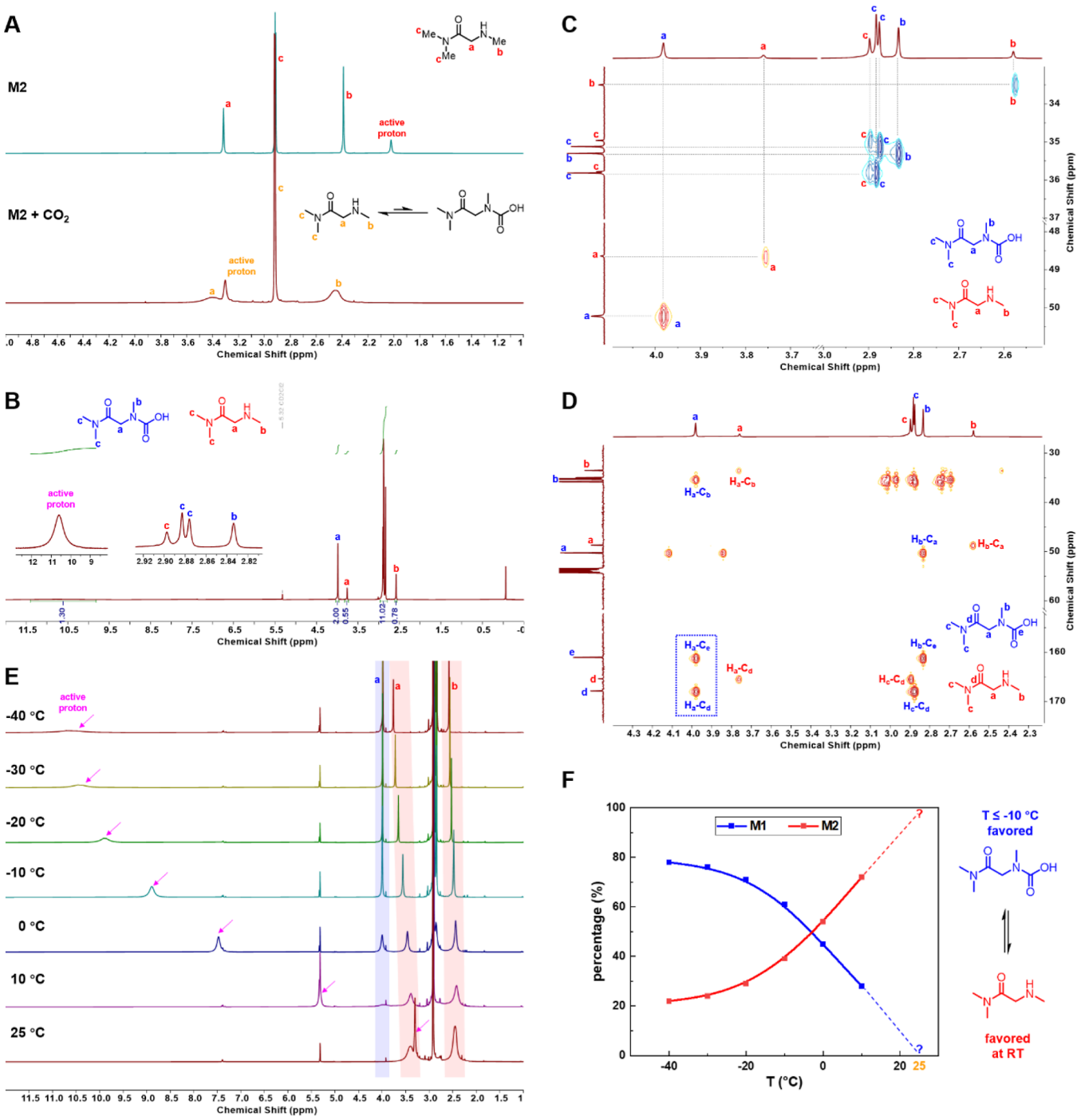

Figure 8. (A) ^{1}H NMR spectra of M2 before and after equilibration with CO_2 at RT in DCM-d_2. (B) ^{1}H NMR spectrum of the equilibrium system at −40 °C. (C) HSQC NMR spectrum of the equilibrium system at −40 °C. (D) HMBC NMR spectrum of the equilibrium system at −40 °C. (E) Overlay of ^{1}H NMR spectra of the equilibrium system at different temperatures. (F) Percentage of M1 and M2 calculated from (E).

entry 5 and 6 of Table 2, the finished solution of NBG_{20} (Table 2, entry 1) and NBG_{1000} (Table 2, entry 3) was directly used for the construction of block copolymers via the sequential monomer addition method. Finally, well-defined triblock copolymer NBG_{20}-*b*-Sar_{400}-*b*-NBG_{20} (Figures S17 and S18) and HMW diblock copolymer NBG_{1000}-*b*-Sar_{1000} (Figure S19) were successfully obtained.

2.5. Mechanism Study on Carboxylic Acid-Catalyzed ROP of Sar-NCA. Next, the acid-catalyzed ROP of SarNCA at different temperatures was conducted at a fixed $[M]_0/[I]_0/[A]_0$ ratio of 200:1:5, which all gave good first-order kinetics (Figure 6A, Table S5) and an apparent activation energy (E_a) of 9 ± 1 kcal/mol through the linear fitting of an Arrhenius plot (Figure 6B). To obtain the kinetic isotopic effect (KIE) of our ROP system, the active protons of the initiator benzylamine and acetic acid were all deuterated before polymerization (Figure 6C). At a fixed $[M]_0/[I]_0/[A]_0$ ratio of 200:1:5, the apparent rate constant $k_{D,obs}$ was determined as $(49.1 \pm 0.5) \times 10^{-4}$ s^{-1} (Figures 6C and S20), which gave a KIE value of 1.6. As there are many different elementary reactions coupled together in the acid-catalyzed ROP (Figure S21), the determination of apparent E_a and KIE did not offer

https://doi.org/10.1021/jacs.3c14740
J. Am. Chem. Soc. 2024, 146, 5678−5692

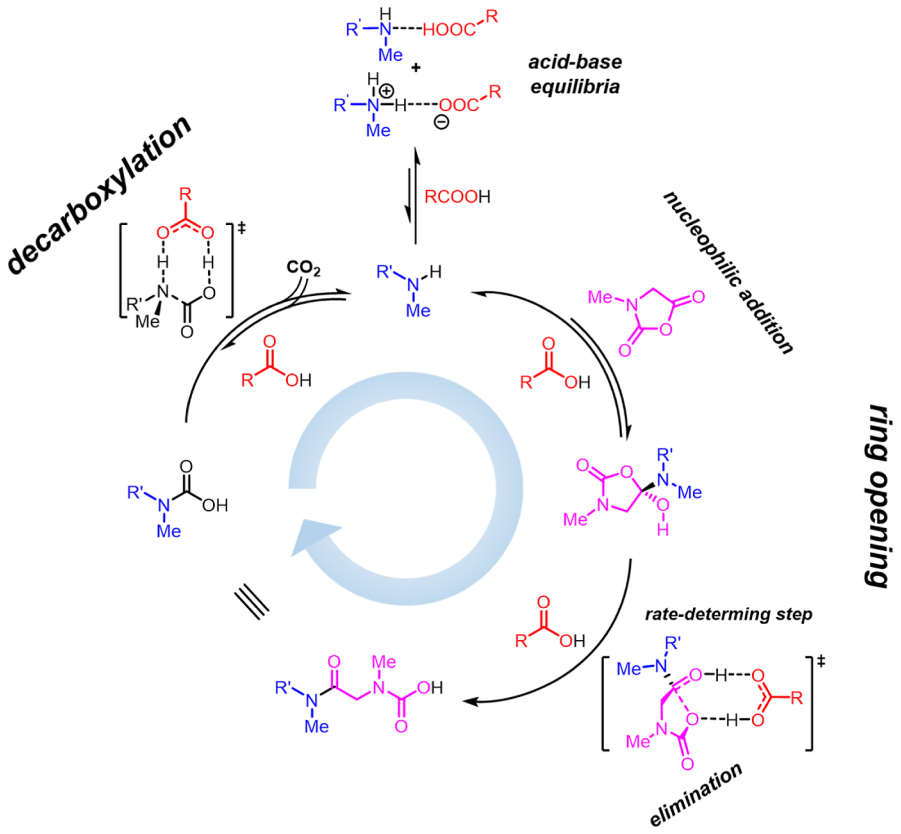

Figure 9. Proposed mechanism for ROP of Sar-NCA catalyzed by carboxylic acids.

accurate information regarding the TSs and potential energy surface (PES). However, these experimental results supported the notion of a proton-transfer-related process likely involved in the RDS for the carboxylic acid-catalyzed ROP of NCA.

Next, we turned to computational studies, DFT calculations specifically, based on model chain propagation reactions between Sar-NCA and dimethylamine, the equivalent of the living chain end (Figure 7A). According to the kinetically observed first-order kinetics, the ring-opening reaction between amine living center and NCA, instead of decarboxylation, was determined as the RDS of the chain propagation, which was then calculated first. For both the noncatalyzed and the acetic acid (AcOH)-catalyzed systems, the ring-opening step could proceed similarly in a stepwise fashion involving the classical nucleophilic addition−elimination process via a tetrahedral intermediate or through a concerted mechanism in one elementary reaction (Figures 7A and S22A).[40,47,63] For the uncatalyzed system, DFT calculations revealed a favorable result of the concerted pathway (path B) over the stepwise pathway (path A), with the activation free energy ($\Delta G^{\ddagger}$) of 20.1 (TSb1) and 36.0 (TSa1) kcal/mol, respectively (Figures 7A and S22B). For the acid-catalyzed system (Figure 7A, path C), the introduction of a carboxylic acid catalyst distinctly reshaped the PES in the stepwise route, yielding a substantially lower energy barrier $\Delta G^{\ddagger}$ of only 11.4 kcal/mol (Figure 7A). Remarkably, AcOH played a crucial role as a bifunctional catalyst throughout the ring-opening process. In TSc1, the hydrogen bonding between the carbonyl lone pair of AcOH and dimethylamine enhances the nucleophilicity of the amine; in the meantime, the transferring carboxylic proton stabilizes the developing negative charge on the oxygen atom of the NCA carbonyl being attacked. After the formation of the unstable intermediate INTc1, it undergoes a series of low-barrier processes to give the tetrahedral intermediate INTc3 with a slightly higher energy. Next, in INTc3, the carbonyl oxygen and acidic hydrogen of AcOH combine with the hydroxyl and the leaving carboxyl oxygen, respectively, and simultaneously activate the elimination-driven hydroxyl oxygen lone pair and leaving group, preparing for the next elimination TS TSc3. TSc3 was found to be the rate-determining TS (11.4 kcal/mol) for the ring-opening stage in path C, being 24.6 and 8.7 kcal/mol lower than path A and B without acid catalysis. After several consecutive low-barrier TS and INT, the carbamic acid intermediate M1 was produced, and the catalyst AcOH was regenerated. The TS for the acid-catalyzed concerted pathway (Figure S22A, path D), however, could not be located.

To understand the linear relationship of k_{obs} and catalyst pK_a observed in Figure 4A,B, additional calculations were performed on RDS TSc3 using acids of different pK_a to decouple the effects of acid−amine equilibrium[64,65] and the catalytic activity (Figure 7B). Interestingly, while the tendency to form the hydrogen-bond complex (HC) (ΔG_{hc}) of acid and amine was negatively correlated with pK_a of the catalysts, the catalytic barrier $\Delta G^{\ddagger}$ of these catalysts was almost identical, in the range of 11.1−11.4 kcal/mol (Figure 7C, Tables S6 and S7). This result indicated that the catalytic activities of carboxylic acids were not sensitive to their acidities, and the pK_a-dependent kinetics mainly resulted from the acid−amine equilibrium. The weaker the acid, the less the tendency for the formation of the acid−amine complex, the faster the ROP. Interestingly, during the calculation, 2-hydroxypyridine was also predicted to facilitate the elimination of the tetrahedral

https://doi.org/10.1021/jacs.3c14740
J. Am. Chem. Soc. 2024, 146, 5678−5692

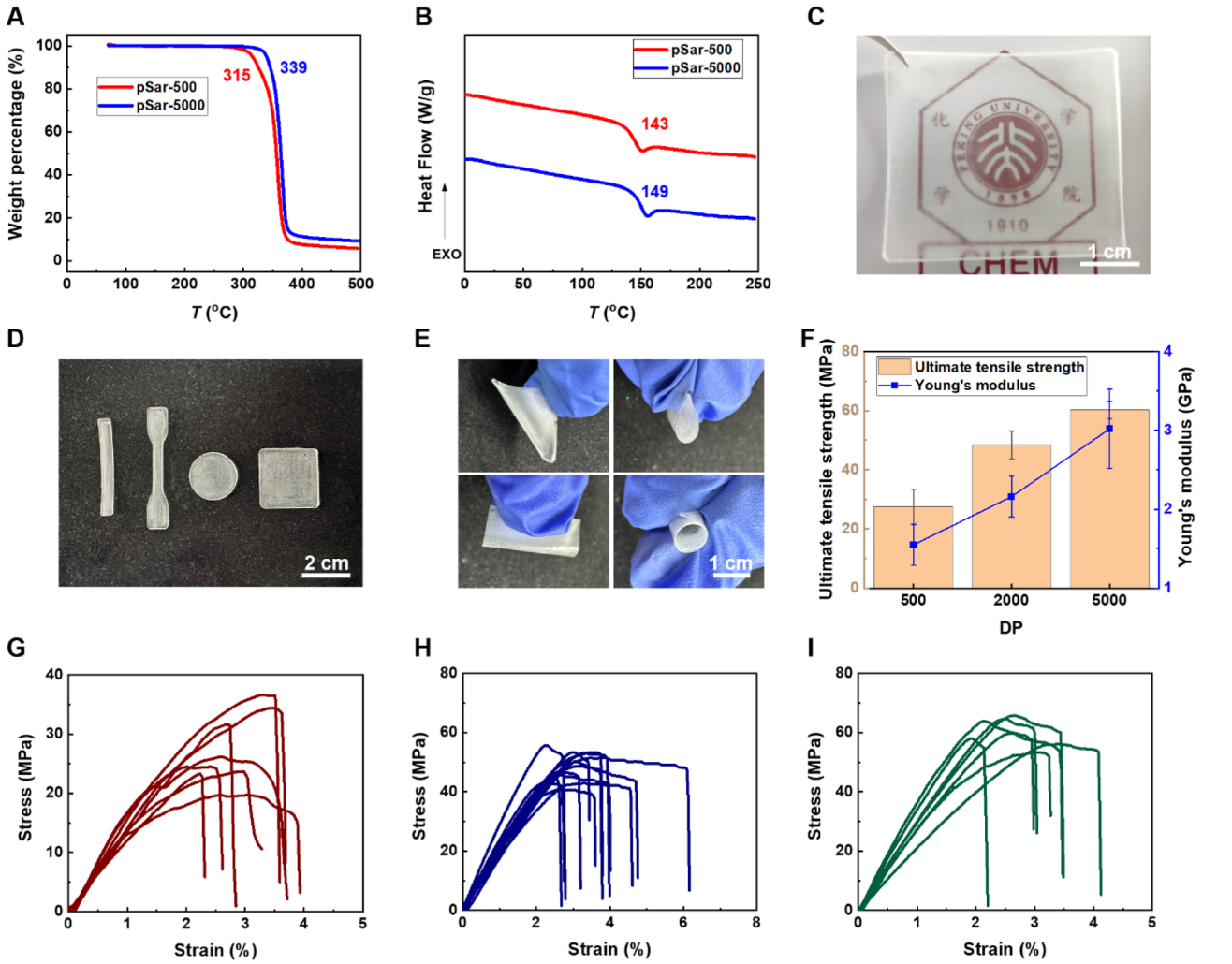

Figure 10. Material properties of HMW pSar. (A) TGA curves of $pSar_{500}$ and $pSar_{5000}$. (B) DSC curves of $pSar_{500}$ and $pSar_{5000}$. (C) Photograph of $pSar_{5000}$ as a transparent film (4.0 cm × 3.5 cm × 92 μm) (the background logo reprinted with permission from Peking University). (D) Shaped pSar bulk materials produced by solution casting. (E) pSar films under bending. (F) Dependence of ultimate tensile strength and Young's modulus of pSar films on DP. (G) Tensile stress−strain curves of $pSar_{500}$. (H) Tensile stress−strain curves of $pSar_{2000}$. (I) Tensile stress−strain curves of $pSar_{5000}$.

intermediate (Table S7 and Figure S23), whose catalytic activity was further proved by experiments (Figure S24).

For decarboxylation, the noncatalyzed intramolecular route and the acid-assisted intermolecular proton transfer route were examined by DFT calculation (Figure 7D). The free energy of the highly strained four-member-ring TSa2 was calculated as 30.6 kcal/mol, which corresponds to an unfavorable energy barrier $\Delta G^{\ddagger}$ of 37.3 kcal/mol starting from M1. With the catalysis of AcOH, however, the decarboxylation proceeded through a concerted eight-membered-ring TS (TSc5) with the ∠N−H−O and ∠O−H−O being 176.4 and 174.1°, respectively. Compared with TSa2 with a ∠N−H−O of 112.4°, the near linear proton transfer geometry of TSc5 was more favorable, which likely rendered the latter with a significantly reduced $\Delta G^{\ddagger}$ (13.4 kcal/mol). It is worth mentioning that the energy of the decarboxylated intermediate M2 was calculated to be significantly higher than that of M1 with a carbamic acid (3.0 vs −6.7 kcal/mol), predicting the decarboxylation to be thermodynamically highly unfavorable.

To verify the relative stability of M1 and M2 experimentally, the deuterated DCM solution of *N*,*N*-dimethyl-2-(methylamino)acetamide (M2) was equilibrated in a sealed NMR tube filled with 1 atm of CO_2 and monitored by in situ NMR. At RT (25 °C), the complete disappearance of M2 signals and significant broadening of peaks in both ^{1}H and ^{13}C NMR spectra suggested the coexistence of various species or conformers and their interconversion at a time scale of NMR detection (Figures 8A, S25). Then the temperature was cooled to −40 °C to freeze the fast interconversions, from which two sets of sharp peaks emerged for both ^{1}H and ^{13}C NMR spectra (Figures 8B and S26). Further 2D NMR experiments, namely, HSQC and HMBC (Figure 8C,D), observed strong correlation signals between α-H ($H_{a,blue}$) and two carbonyl carbon atoms ($C_{d,blue}$ and $C_{e,blue}$), providing crucial evidence for the formation of carbamic acid M1.[66] As a result, M1 was assigned to be the main component of the system at −40 °C, accounting for 78%, while the minor peaks were assigned to amine M2. Consecutive monitoring of the ^{1}H NMR spectra from −40 °C to RT depicted the gradual decomposition of M1 and broadening of peaks (Figure 8E). The distribution of M1 and M2 was then calculated through the integration of sarcosine α-H, revealing a temperature-dependent stability of M1 (Figure 8F). At 10 °C, M1 (%) reached 28%, while no significant peaks of M1 were found at RT. Additionally, the

https://doi.org/10.1021/jacs.3c14740
J. Am. Chem. Soc. 2024, 146, 5678−5692

chemical shift of active proton also shifted from 10.6 to 3.3 ppm, consistent with the growing percentage of amine M2 (Figure 8E). Based on the above NMR result, a brief conclusion could be made that under the atmosphere of CO_2, carbamic acid M1 was more stable than amine M2 at low temperatures ($T \leq -10$ °C).[67] At RT, rapid interconversion existed between M1 and M2, leading to peak broadening in NMR and chain growth inhibition and reactivation, respectively. The discrepancy of DFT and experiments, however, could be partly attributed to the absence of specific solvent−solute interactions under the implicit solvent model, as the acidic proton of DCM was also reported to exhibit hydrogen-bond propensities.[68]

Taking together the DFT and experimental results, we proposed the following catalytic cycle of the carboxylic acid-enhanced ROP of Sar-NCA (Figures 9 and S27). To begin with, the secondary amine living center was in fast equilibria with carboxylic acids and CO_2. Due to the relative low stability of carbamic acid at RT, the CO_2 equilibrium had little influence on the concentration of amine, which was actually controlled by the acid−amine equilibria. The nucleophilic addition of amine to NCA was reversible, forming the high-energy tetrahedral intermediate, whose elimination is the RDS for the overall chain growth process according to DFT. The experimental result determined low apparent E_a (Figure 6B), agreeing well with the DFT-calculated $\Delta G^{\ddagger}$ of TSc3 (Figure 7A).[69] In the elimination TS, the proton of the carboxylic acid binds to the leaving carboxyl group and the carbonyl oxygen binds to the hydroxyl group, simultaneously activating the lone pair and the leaving group for facilitated elimination. After elimination, unstable carbamic acid species were generated and their decarboxylation led to new amine living centers. The interconversion of the M1 and M2 as predicted by DFT and observed by NMR (Figures 7D and 8), on the other hand, offered interesting implications regarding the kinetics of the noncatalyzed ROP of Sar-NCA, in which an induction period followed by a self-acceleration stage was observed experimentally (Figures 3A and S7). It was proposed that the induction period represented the slow uncatalyzed ring-opening reaction between amine and NCA, which was predicted by DFT to have a high activation barrier (Figure 7A, path B). As the reaction continued, more and more CO_2 was produced through the decarboxylation of resulting carbamic acids. Once the CO_2−amine equilibrium was established, i.e., the concentration of the CO_2 accumulated to a certain amount, the ROP would probably be self-catalyzed by the carbamic acids, resulting in the self-acceleration in the second stage (increasing $[CO_2]$) and near first-order kinetics in the third stage (steady $[CO_2]$) (Figures S7 and S28). Indeed, further DFT calculations indicated that the model carbamic acid Me_2NCOOH possessed comparable catalytic activities to acetic acid in both ring-opening and decarboxylation steps (Figures S29 and S30). In contrast, the addition of carboxylic acid bypassed the initial induction period and provided a much higher catalyst concentration and thus led to the significantly accelerated kinetics (up to 50-fold).

2.6. Molecular Weight-Dependent Thermal and Mechanical Properties of pSar. The thermal and mechanical properties of pSar were examined, which were rarely explored before. With the ability to obtain UHMW pSar, here, we synthesized pSar samples on gram scales with targeted DP of 500, 2000, and 5000, respectively (Table S8, Figure S31), and paid special attention to the MW-dependent performances. The 5% weight loss thermal decomposition temperature (T_d), measured by thermogravimetric analysis (TGA), of $pSar_{500}$ and $pSar_{5000}$ was 315 and 339 °C, respectively (Figure 10A), both significantly higher than 250 °C, the previously reported number of $pSar_{100}$.[70] The glass transition temperature (T_g), determined with differential scanning calorimetry (DSC), of $pSar_{500}$ and $pSar_{5000}$ was measured to be 143 and 149 °C, respectively (Figure 10B), similar to the 143 °C value reported in the literature. All $pSar_{500}$, $pSar_{2000}$, and $pSar_{5000}$ samples were soluble in water at a concentration greater than or equal to 100 mg/mL. Using the solution casting method, pSar of the above MWs was fabricated into transparent, smooth, thin films, as well as other shaped bulk materials with excellent flexibility (Figure 10C−E). The pSar films exhibited good mechanical strength in uniaxial tensile experiments (Figure 10F−I), with a characteristic MW dependence on both the ultimate tensile strength and Young's modulus (Figure 10F). Specifically, the $pSar_{5000}$ samples gave an ultimate tensile strength of (60.2 ± 3.0) MPa and Young's modulus of (3.0 ± 0.5) GPa, both greater than those of $pSar_{500}$ and $pSar_{2000}$ (Figure 10F). Interestingly, the mechanical properties of all pSar films showed moisture responsiveness in a 70% humidity environment, with decreased ultimate tensile strengths but markedly increased elongations at break (Figure S32). Additionally, the bending fatigue behavior of the $pSar_{5000}$ film was roughly probed by manually bending the film 40 times continuously, through which no significant failure was observed, demonstrating good fatigue properties (Supporting Information Video). Moreover, pSar could be alternatively manufactured through the thermoforming process under 195 °C to form shaped bulk materials (Figure S33). In summary, the increase in MW greatly improves the thermal stability and mechanical strength of pSar bulk materials, laying the foundation for the subsequent development of pSar-based materials.

3. CONCLUSIONS

This paper reported the controlled/living polymerization of Sar-NCA using carboxylic acids as the catalyst under mild conditions. The method features fast kinetics up to a 50-fold enhancement compared with no acid catalysis, capability of multiple chain extensions, narrow $Đ$ below 1.05, and UHMW of pSar with an obtainable DP up to 8000, 16 folds higher than the current record DP of pSar ever reported. The method also showed good moisture tolerance with no need of air-free conditions or dry solvents for pSar with a targeting DP of 1000 or below. DFT calculations and experiments elucidated the dual role of carboxylic acid in the ROP, both acting as a catalyst and a Brønsted acid inhibitor. For catalysis, carboxylic acid was found to facilitate ROP throughout the nucleophilic addition, elimination (breaking C−O bond, RDS), and decarboxylation steps. More specifically, by mainly serving as both hydrogen-bond donor and acceptor, the introduction of carboxylic acid enabled the proton transfer via more favorable geometries and reduced charge separation of these processes, thereby lowering the energy barrier significantly. The inhibition effects of carboxylic acids, however, were significant only for the catalyst with high acidity or with high acid loading. HMW pSar exhibited enhanced thermal and mechanical properties superior to its LMW counterparts and can be easily processed. Moreover, the monomer scope of this method can be extended to other NNCAs, such as NBG-NCA, for the synthesis of HMW (block) (co)polypeptoids. This work

https://doi.org/10.1021/jacs.3c14740
J. Am. Chem. Soc. 2024, 146, 5678−5692

greatly enriched the basic understanding of Sar-NCA polymerization, highlighted the importance of proton transfer for NCA ROP in general, and provided a simple yet highly practical route to pSar of various MWs and for diverse applications.

■ ASSOCIATED CONTENT

Supporting Information

The Supporting Information is available free of charge at https://pubs.acs.org/doi/10.1021/jacs.3c14740.

Materials, instrumentation, synthesis of Sar-NCA, typical procedure of the benzoic acid-catalyzed ROP of Sar-NCA, typical procedure of kinetic studies, typical procedure of pivalic acid-catalyzed consecutive chain extensions, synthesis of NBG-NCA, typical procedure of pivalic acid-catalyzed ROP of NBG-NCA and the synthesis of (multi) block copolymers, synthesis of deuterated benzylamine ($PhCH_2ND_2$), procedure of the equilibrium experiment of N,N-dimethyl-2-(methylamino)acetamide (M2) and CO_2, DFT study, typical procedure of pSar processing by the solution casting method, typical procedure of pSar processing by the thermoforming method, and other supplementary data (PDF)

Video showing the $pSar_{5000}$ film being bended 40 times to probe its bending fatigue behavior (MP4)

■ AUTHOR INFORMATION

Corresponding Author

Hua Lu − *Beijing National Laboratory for Molecular Sciences, Center for Soft Matter Science and Engineering, Key Laboratory of Polymer Chemistry and Physics of Ministry of Education, College of Chemistry and Molecular Engineering, Peking University, Beijing 100871, China;* orcid.org/0000-0003-2180-3091; Email: chemhualu@pku.edu.cn

Authors

Shuo Wang − *Beijing National Laboratory for Molecular Sciences, Center for Soft Matter Science and Engineering, Key Laboratory of Polymer Chemistry and Physics of Ministry of Education, College of Chemistry and Molecular Engineering, Peking University, Beijing 100871, China;* orcid.org/0000-0002-1380-5890

Ming-Yuan Lu − *Beijing National Laboratory for Molecular Sciences, Center for Soft Matter Science and Engineering, Key Laboratory of Polymer Chemistry and Physics of Ministry of Education, College of Chemistry and Molecular Engineering, Peking University, Beijing 100871, China*

Si-Kang Wan − *Engineering Research Center of Advanced Rare Earth Materials (Ministry of Education), Department of Chemistry, Tsinghua University, Beijing 100084, China*

Chun-Yan Lyu − *Beijing National Laboratory for Molecular Sciences, Center for Soft Matter Science and Engineering, Key Laboratory of Polymer Chemistry and Physics of Ministry of Education, College of Chemistry and Molecular Engineering, Peking University, Beijing 100871, China*

Zi-You Tian − *Beijing National Laboratory for Molecular Sciences, Center for Soft Matter Science and Engineering, Key Laboratory of Polymer Chemistry and Physics of Ministry of Education, College of Chemistry and Molecular Engineering, Peking University, Beijing 100871, China*

Kai Liu − *Engineering Research Center of Advanced Rare Earth Materials (Ministry of Education), Department of Chemistry, Tsinghua University, Beijing 100084, China;* orcid.org/0000-0003-0878-5191

Complete contact information is available at: https://pubs.acs.org/10.1021/jacs.3c14740

Notes

The authors declare no competing financial interest.

■ ACKNOWLEDGMENTS

This work was supported by the National Natural Science Foundation of China (22125101 and 22331002), Beijing Natural Science Foundation (2220023), and Li Ge-Zhao Ning Life Science Youth Research Fund. We thank Prof. Shi-Yong Liu (USTC) and Prof. Rong Zhu (PKU) for constructive discussions and thank Dr. Hui Fu, Xiu Zhang, and Li-Juan Wang (PKUAIC) for NMR characterization.

■ REFERENCES

(1) Birke, A.; Ling, J.; Barz, M. Polysarcosine-containing copolymers: Synthesis, characterization, self-assembly, and applications. *Prog. Polym. Sci.* **2018**, *81*, 163−208.

(2) Weber, B.; Birke, A.; Fischer, K.; Schmidt, M.; Barz, M. Solution Properties of Polysarcosine: From Absolute and Relative Molar Mass Determinations to Complement Activation. *Macromolecules* **2018**, *51*, 2653−2661.

(3) Lau, K. H. A.; Ren, C.; Sileika, T. S.; Park, S. H.; Szleifer, I.; Messersmith, P. B. Surface-Grafted Polysarcosine as a Peptoid Antifouling Polymer Brush. *Langmuir* **2012**, *28*, 16099−16107.

(4) Hu, Y.; Hou, Y.; Wang, H.; Lu, H. Polysarcosine as an Alternative to PEG for Therapeutic Protein Conjugation. *Bioconjugate Chem.* **2018**, *29*, 2232−2238.

(5) Nogueira, S. S.; Schlegel, A.; Maxeiner, K.; Weber, B.; Barz, M.; Schroer, M. A.; Blanchet, C. E.; Svergun, D. I.; Ramishetti, S.; Peer, D.; Langguth, P.; Sahin, U.; Haas, H. Polysarcosine-Functionalized Lipid Nanoparticles for Therapeutic mRNA Delivery. *ACS Appl. Nano Mater.* **2020**, *3*, 10634−10645.

(6) Bi, D.; Unthan, D. M.; Hu, L.; Bussmann, J.; Remaut, K.; Barz, M.; Zhang, H. Polysarcosine-based lipid formulations for intracranial delivery of mRNA. *J. Controlled Release* **2023**, *356*, 1−13.

(7) Kidchob, T.; Kimura, S.; Imanishi, Y. Amphiphilic poly(Ala)-b-poly(Sar) microspheres loaded with hydrophobic drug. *J. Controlled Release* **1998**, *51*, 241−248.

(8) Makino, A.; Kizaka-Kondoh, S.; Yamahara, R.; Hara, I.; Kanzaki, T.; Ozeki, E.; Hiraoka, M.; Kimura, S. Near-infrared fluorescence tumor imaging using nanocarrier composed of poly(l-lactic acid)-block-poly(sarcosine) amphiphilic polydepsipeptide. *Biomaterials* **2009**, *30*, 5156−5160.

(9) Birke, A.; Huesmann, D.; Kelsch, A.; Weilbächer, M.; Xie, J.; Bros, M.; Bopp, T.; Becker, C.; Landfester, K.; Barz, M. Polypeptoid-block-polypeptide Copolymers: Synthesis, Characterization, and Application of Amphiphilic Block Copolypept(o)ides in Drug Formulations and Miniemulsion Techniques. *Biomacromolecules* **2014**, *15*, 548−557.

(10) Deng, Y.; Zou, T.; Tao, X.; Semetey, V.; Trepout, S.; Marco, S.; Ling, J.; Li, M.-H. Poly(ε-caprolactone)-block-polysarcosine by Ring-Opening Polymerization of Sarcosine N-Thiocarboxyanhydride: Synthesis and Thermoresponsive Self-Assembly. *Biomacromolecules* **2015**, *16*, 3265−3274.

(11) Miao, Y.; Xie, F.; Cen, J.; Zhou, F.; Tao, X.; Luo, J.; Han, G.; Kong, X.; Yang, X.; Sun, J.; Ling, J. Fe3+@polyDOPA-b-polysarcosine, a T1-Weighted MRI Contrast Agent via Controlled NTA Polymerization. *ACS Macro Lett.* **2018**, *7*, 693−698.

(12) Varlas, S.; Georgiou, P. G.; Bilalis, P.; Jones, J. R.; Hadjichristidis, N.; O'Reilly, R. K. Poly(sarcosine)-Based Nano-Objects with Multi-Protease Resistance by Aqueous Photoinitiated Polymerization-Induced Self-Assembly (Photo-PISA). *Biomacromolecules* **2018**, *19*, 4453−4462.

(13) Bauer, T. A.; Imschweiler, J.; Muhl, C.; Weber, B.; Barz, M. Secondary Structure-Driven Self-Assembly of Thiol-Reactive Polypept(o)ides. *Biomacromolecules* **2021**, *22*, 2171−2180.
(14) Kincaid, J. R. A.; Wong, M. J.; Akporji, N.; Gallou, F.; Fialho, D. M.; Lipshutz, B. H. Introducing Savie: A Biodegradable Surfactant Enabling Chemo- and Biocatalysis and Related Reactions in Recyclable Water. *J. Am. Chem. Soc.* **2023**, *145*, 4266−4278.
(15) Kricheldorf, H. R.; von Lossow, C.; Schwarz, G. Primary Amine-Initiated Polymerizations of Alanine-NCA and Sarcosine-NCA. *Macromol. Chem. Phys.* **2004**, *205*, 918−924.
(16) Fetsch, C.; Grossmann, A.; Holz, L.; Nawroth, J. F.; Luxenhofer, R. Polypeptoids from N-Substituted Glycine N-Carboxyanhydrides: Hydrophilic, Hydrophobic, and Amphiphilic Polymers with Poisson Distribution. *Macromolecules* **2011**, *44*, 6746−6758.
(17) Doriti, A.; Brosnan, S. M.; Weidner, S. M.; Schlaad, H. Synthesis of polysarcosine from air and moisture stable N-phenoxycarbonyl-N-methylglycine assisted by tertiary amine base. *Polym. Chem.* **2016**, *7*, 3067−3070.
(18) Salas-Ambrosio, P.; Tronnet, A.; Since, M.; Bourgeade-Delmas, S.; Stigliani, J.-L.; Vax, A.; Lecommandoux, S.; Dupuy, B.; Verhaeghe, P.; Bonduelle, C. Cyclic Poly(α-peptoid)s by Lithium bis-(trimethylsilyl)amide (LiHMDS)-Mediated Ring-Expansion Polymerization: Simple Access to Bioactive Backbones. *J. Am. Chem. Soc.* **2021**, *143*, 3697−3702.
(19) Chen, K.; Wu, Y.; Wu, X.; Zhou, M.; Zhou, R.; Wang, J.; Xiao, X.; Yuan, Y.; Liu, R. Facile synthesis of polypeptoids bearing bulky sidechains via urea accelerated ring-opening polymerization of α-amino acid N-substituted N-carboxyanhydrides. *Polym. Chem.* **2022**, *13*, 420−426.
(20) Rasines Mazo, A.; Allison-Logan, S.; Karimi, F.; Chan, N. J.-A.; Qiu, W.; Duan, W.; O'Brien-Simpson, N. M.; Qiao, G. G. Ring opening polymerization of α-amino acids: advances in synthesis, architecture and applications of polypeptides and their hybrids. *Chem. Soc. Rev.* **2020**, *49*, 4737−4834.
(21) Hadjichristidis, N.; Iatrou, H.; Pitsikalis, M.; Sakellariou, G. Synthesis of Well-Defined Polypeptide-Based Materials via the Ring-Opening Polymerization of α-Amino Acid N-Carboxyanhydrides. *Chem. Rev.* **2009**, *109*, 5528−5578.
(22) Deming, T. J. Facile synthesis of block copolypeptides of defined architecture. *Nature* **1997**, *390*, 386−389.
(23) Dimitrov, I.; Schlaad, H. Synthesis of nearly monodisperse polystyrene-polypeptide block copolymers via polymerisation of N-carboxyanhydrides. *Chem. Commun.* **2003**, 2944−2945.
(24) Lu, H.; Cheng, J. Hexamethyldisilazane-Mediated Controlled Polymerization of α-Amino Acid N-Carboxyanhydrides. *J. Am. Chem. Soc.* **2007**, *129*, 14114−14115.
(25) Conejos-Sánchez, I.; Duro-Castano, A.; Birke, A.; Barz, M.; Vicent, M. J. A controlled and versatile NCA polymerization method for the synthesis of polypeptides. *Polym. Chem.* **2013**, *4*, 3182−3186.
(26) Zhao, W.; Lv, Y.; Li, J.; Feng, Z.; Ni, Y.; Hadjichristidis, N. Fast and selective organocatalytic ring-opening polymerization by fluorinated alcohol without a cocatalyst. *Nat. Commun.* **2019**, *10*, 3590.
(27) Song, Z.; Fu, H.; Wang, J.; Hui, J.; Xue, T.; Pacheco, L. A.; Yan, H.; Baumgartner, R.; Wang, Z.; Xia, Y.; Wang, X.; Yin, L.; Chen, C.; Rodríguez-López, J.; Ferguson, A. L.; Lin, Y.; Cheng, J. Synthesis of polypeptides via bioinspired polymerization of in situ purified N-carboxyanhydrides. *Proc. Natl. Acad. Sci. U.S.A.* **2019**, *116*, 10658−10663.
(28) Wu, Y.; Chen, K.; Wu, X.; Liu, L.; Zhang, W.; Ding, Y.; Liu, S.; Zhou, M.; Shao, N.; Ji, Z.; Chen, J.; Zhu, M.; Liu, R. Superfast and Water-Insensitive Polymerization on α-Amino Acid N-Carboxyanhydrides to Prepare Polypeptides Using Tetraalkylammonium Carboxylate as the Initiator. *Angew. Chem., Int. Ed.* **2021**, *60*, 26063−26071.
(29) Li, K.; Li, Z.; Shen, Y.; Fu, X.; Chen, C.; Li, Z. Organobase 1,1,3,3-tetramethyl guanidine catalyzed rapid ring-opening polymerization of α-amino acid N-carboxyanhydrides adaptive to amine, alcohol and carboxyl acid initiators. *Polym. Chem.* **2022**, *13*, 586−591.
(30) Lv, W.; Wang, Y.; Li, M.; Wang, X.; Tao, Y. Precision Synthesis of Polypeptides via Living Anionic Ring-Opening Polymerization of N-Carboxyanhydrides by Tri-thiourea Catalysts. *J. Am. Chem. Soc.* **2022**, *144*, 23622−23632.
(31) Kricheldorf, H. R.; Sell, M.; Schwarz, G. Primary Amine-Initiated Polymerizations of α-Amino Acid N-Thiocarbonic Acid Anhydrosulfide. *J. Macromol. Sci., Part A: Pure Appl. Chem.* **2008**, *45*, 425−430.
(32) Tao, X.; Zheng, B.; Kricheldorf, H. R.; Ling, J. Are N-substituted glycine N-thiocarboxyanhydride monomers really hard to polymerize? *J. Polym. Sci., Part A: Polym. Chem.* **2017**, *55*, 404−410.
(33) Tao, X.; Zheng, B.; Bai, T.; Li, M.-H.; Ling, J. Polymerization of N-Substituted Glycine N-Thiocarboxyanhydride through Regioselective Initiation of Cysteamine: A Direct Way toward Thiol-Capped Polypeptoids. *Macromolecules* **2018**, *51*, 4494−4501.
(34) Zheng, B.; Xu, S.; Ni, X.; Ling, J. Understanding Acid-Promoted Polymerization of the N-Substituted Glycine N-Thiocarboxyanhydride in Polar Solvents. *Biomacromolecules* **2021**, *22*, 1579−1589.
(35) Siefker, D.; Chan, B. A.; Zhang, M.; Nho, J.-W.; Zhang, D. 1,1,3,3-Tetramethylguanidine-Mediated Zwitterionic Ring-Opening Polymerization of Sarcosine-Derived N-Thiocarboxyanhydride toward Well-Defined Polysarcosine. *Macromolecules* **2022**, *55*, 2509−2516.
(36) Siefker, D.; Williams, A. Z.; Stanley, G. G.; Zhang, D. Organic Acid Promoted Controlled Ring-Opening Polymerization of α-Amino Acid-Derived N-thiocarboxyanhydrides (NTAs) toward Well-defined Polypeptides. *ACS Macro Lett.* **2018**, *7*, 1272−1277.
(37) Hou, Y.; Lu, H. Protein PEPylation: A New Paradigm of Protein-Polymer Conjugation. *Bioconjugate Chem.* **2019**, *30*, 1604−1616.
(38) Cheng, G.-J.; Zhang, X.; Chung, L. W.; Xu, L.; Wu, Y.-D. Computational Organic Chemistry: Bridging Theory and Experiment in Establishing the Mechanisms of Chemical Reactions. *J. Am. Chem. Soc.* **2015**, *137*, 1706−1725.
(39) Scheiner, S. Theoretical studies of proton transfers. *Acc. Chem. Res.* **1985**, *18*, 174−180.
(40) Liu, J.; Ling, J. DFT Study on Amine-Mediated Ring-Opening Mechanism of α-Amino Acid N-Carboxyanhydride and N-Substituted Glycine N-Carboxyanhydride: Secondary Amine versus Primary Amine. *J. Phys. Chem. A* **2015**, *119*, 7070−7074.
(41) Wang, L.; Zipse, H. Bifunctional Catalysis of Ester Aminolysis - A Computational and Experimental Study. *Liebigs Ann.* **1996**, *1996*, 1501−1509.
(42) Duan, X.; Scheiner, S. Energetics, proton transfer rates, and kinetic isotope effects in bent hydrogen bonds. *J. Am. Chem. Soc.* **1992**, *114*, 5849−5856.
(43) Nguyen Minh, T.; Ha, T. K. A theoretical study of the formation of carbonic acid from the hydration of carbon dioxide: a case of active solvent catalysis. *J. Am. Chem. Soc.* **1984**, *106*, 599−602.
(44) Williams, I. H.; Spangler, D.; Femec, D. A.; Maggiora, G. M.; Schowen, R. L. Theoretical models for solvation and catalysis in carbonyl addition. *J. Am. Chem. Soc.* **1983**, *105*, 31−40.
(45) Williams, I. H. Theoretical modelling of specific solvation effects upon carbonyl addition. *J. Am. Chem. Soc.* **1987**, *109*, 6299−6307.
(46) Ilieva, S.; Galabov, B.; Musaev, D. G.; Morokuma, K.; Schaefer, H. F. Computational Study of the Aminolysis of Esters. The Reaction of Methylformate with Ammonia. *J. Org. Chem.* **2003**, *68*, 1496−1502.
(47) Petrova, T.; Okovytyy, S.; Gorb, L.; Leszczynski, J. Computational Study of the Aminolysis of Anhydrides: Effect of the Catalysis to the Reaction of Succinic Anhydride with Methylamine in Gas Phase and Nonpolar Solution. *J. Phys. Chem. A* **2008**, *112*, 5224−5235.
(48) Hu, Y.; Tian, Z.-Y.; Xiong, W.; Wang, D.; Zhao, R.; Xie, Y.; Song, Y.-Q.; Zhu, J.; Lu, H. Water-Assisted and Protein-Initiated Fast and Controlled Ring-Opening Polymerization of Proline N-Carboxyanhydride. *Natl. Sci. Rev.* **2022**, *9*, nwac033.
(49) Jehanno, C.; Mezzasalma, L.; Sardon, H.; Ruipérez, F.; Coulembier, O.; Taton, D. Benzoic Acid as an Efficient Organo-

https://doi.org/10.1021/jacs.3c14740
J. Am. Chem. Soc. 2024, 146, 5678−5692

catalyst for the Statistical Ring-Opening Copolymerization of ε-Caprolactone and L-Lactide: A Computational Investigation. *Macromolecules* **2019**, *52*, 9238−9247.
(50) da Silva, G. Carboxylic Acid Catalyzed Keto-Enol Tautomerizations in the Gas Phase. *Angew. Chem., Int. Ed.* **2010**, *49*, 7523−7525.
(51) Kim, Y. Direct Dynamics Calculation for the Double Proton Transfer in Formic Acid Dimer. *J. Am. Chem. Soc.* **1996**, *118*, 1522−1528.
(52) Lim, J.-H.; Lee, E. K.; Kim, Y. Theoretical Study for Solvent Effect on the Potential Energy Surface for the Double Proton Transfer in Formic Acid Dimer and Formamidine Dimer. *J. Phys. Chem. A* **1997**, *101*, 2233−2239.
(53) Feng, G.; Favero, L. B.; Maris, A.; Vigorito, A.; Caminati, W.; Meyer, R. Proton Transfer in Homodimers of Carboxylic Acids: The Rotational Spectrum of the Dimer of Acrylic Acid. *J. Am. Chem. Soc.* **2012**, *134*, 19281−19286.
(54) Ballard, D. G. H.; Bamford, C. H. Studies in polymerization -VII. The polymerization of N-carboxy-α-amino acid anhydrides. *Proc. R. Soc. London, Ser. A* **1954**, *223*, 495−520.
(55) Wang, S.; Lu, H. Ring-Opening Polymerization of Amino Acid N-Carboxyanhydrides with Unprotected/Reactive Side Groups. I. d-Penicillamine N-Carboxyanhydride. *ACS Macro Lett.* **2023**, *12*, 555−562.
(56) Yu, X.; Wang, Y.; Dong, Y.; Zhao, N.; Zhang, L.; Xuan, S.; Zhang, Z. Efficient Synthesis of N-Methyl Polypeptides by Organic Acid Promoted Controlled Ring-Opening Polymerization of N-Methyl-α-Amino Acids N-Carboxyanhydrides. *Macromolecules* **2023**, *56*, 8899−8911.
(57) Liu, X.; Huang, J.; Wang, J.; Sheng, H.; Yuan, Z.; Wang, W.; Li, W.; Song, Z.; Cheng, J. Accelerated and controlled polymerization of N-carboxyanhydrides catalyzed by acids. *ChemRxiv* **2023**, DOI: 10.26434/chemrxiv-2023-906jv.
(58) Liang, J.; Zhi, X.; Zhou, Q.; Yang, J. Binaphthol-derived phosphoric acids as efficient organocatalysts for the controlled ring-opening polymerization of γ-benzyl- -glutamate N-carboxyanhydrides. *Polymer* **2019**, *165*, 83−90.
(59) Kamlet, M. J.; Taft, R. W. The solvatochromic comparison method. I. The beta.-scale of solvent hydrogen-bond acceptor (HBA) basicities. *J. Am. Chem. Soc.* **1976**, *98*, 377−383.
(60) Kamlet, M. J.; Abboud, J. L. M.; Abraham, M. H.; Taft, R. W. Linear solvation energy relationships. 23. A comprehensive collection of the solvatochromic parameters, pi.*, alpha., and.beta., and some methods for simplifying the generalized solvatochromic equation. *J. Org. Chem.* **1983**, *48*, 2877−2887.
(61) Komarova, A. O.; Dick, G. R.; Luterbacher, J. S. Diformylxylose as a new polar aprotic solvent produced from renewable biomass. *Green Chem.* **2021**, *23*, 4790−4799.
(62) Kortüm, G.; Vogel, W.; Andrussow, K. Disssociation constants of organic acids in aqueous solution. *Pure Appl. Chem.* **1960**, *1*, 187−536.
(63) Ling, J.; Huang, Y. Understanding the Ring-Opening Reaction of α-Amino Acid N-Carboxyanhydride in an Amine-Mediated Living Polymerization: A DFT Study. *Macromol. Chem. Phys.* **2010**, *211*, 1708−1711.
(64) Yerger, E. A.; Barrow, G. M. Acid-Base Reactions in Non-dissociating Solvents. Acetic Acid and Diethylamine in Carbon Tetrachloride and Chloroform. *J. Am. Chem. Soc.* **1955**, *77*, 4474−4481.
(65) DeTar, D. F.; Novak, R. W. Carboxylic acid-amine equilibria in nonaqueous solvents. *J. Am. Chem. Soc.* **1970**, *92*, 1361−1365.
(66) Masuda, K.; Ito, Y.; Horiguchi, M.; Fujita, H. Studies on the solvent dependence of the carbamic acid formation from ω-(1-naphthyl)alkylamines and carbon dioxide. *Tetrahedron* **2005**, *61*, 213−229.
(67) Aresta, M.; Ballivet-Tkatchenko, D.; Dell'Amico, D. B.; Boschi, D.; Calderazzo, F.; Labella, L.; Bonnet, M. C.; Faure, R.; Marchetti, F. Isolation and structural determination of two derivatives of the elusive carbamic acid. *Chem. Commun.* **2000**, 1099−1100.
(68) Allen, F. H.; Wood, P. A.; Galek, P. T. A. Role of chloroform and dichloromethane solvent molecules in crystal packing: an interaction propensity study. *Acta Crystallogr., Sect. B: Struct. Sci., Cryst. Eng. Mater.* **2013**, *69*, 379−388.
(69) Pacey, P. D. Changing conceptions of activation energy. *J. Chem. Educ.* **1981**, *58*, 612−614.
(70) Fetsch, C.; Luxenhofer, R. Thermal Properties of Aliphatic Polypeptoids. *Polymers* **2013**, *5*, 112−127.

https://doi.org/10.1021/jacs.3c14740
J. Am. Chem. Soc. 2024, 146, 5678−5692